Combustion Science and Technology
Publication details, including instructions for authors and subscription information:
http://www.tandfonline.com/loi/gcst20

Numerical Study for Interaction Between Water Mist and Counterflow Diffusion Flame Over Tsuji Burner

SHIN-SHEN TSA [a] , EN-TING LIU [a] & CHIUN-HSUN CHEN [a]
[a] Department of Mechanical Engineering , National Chiao Tung University , HsinChu, Taiwan, 300, R.O.C
Published online: 06 Apr 2007.

To cite this article: SHIN-SHEN TSA , EN-TING LIU & CHIUN-HSUN CHEN (2001) Numerical Study for Interaction Between Water Mist and Counterflow Diffusion Flame Over Tsuji Burner, Combustion Science and Technology, 167:1, 257-289, DOI: 10.1080/00102200108952184

To link to this article: http://dx.doi.org/10.1080/00102200108952184

Combust. Sci. and Tech., 2001, Vol. 167, pp. 257-289
Reprints available directly from the publisher
Photocopying permitted by license only

Numerical Study for Interaction Between Water Mist and Counterflow Diffusion Flame Over Tsuji Burner

SHIN-SHEN TSA, EN-TING LIU and CHIUN-HSUN CHEN*

Department of Mechanical Engineering, National Chiao Tung University, HsinChu, Taiwan 300, R.O.C

(Received January 30, 2001; In final form May 08, 2001)

The interaction between a water mist and a counterflow diffusion flame over a Tsuji burner is studied numerically. The governing system is comprised of two parts. The gas phase combustion model adopts the one developed by Chen and Weng (1990). For droplets, their motions are described by Newton's second law. The corresponding droplet heat and mass transfer are considered by using empirical correlations. The PSI-Cell model is used to manage the two-phase coupling. The evaporation of droplets through heat absorption from the flame can generate vapor in the flow field. The vapor dilutes both the oxidizer and fuel concentrations, and the heat absorption by phase change lowers the flame temperature. For 50 μm droplets, the envelope flame is extinguished from the forward stagnation area and becomes a wake flame as the mist flow rate increases to 7%. The wake flame no longer exists when the mist flow rate is greater than 15%. The critical values for transition of the envelope flame to a wake flame and complete flame extinction for 80 μm droplets were 4.5% and 10% separately. Under the same mist flow rate, the smaller the droplet sizes, the stronger the flame. The effect of droplet size is studied by changing the droplet size and the corresponding mist flows with the number flow rate constant. The critical sizes for transition of the envelope flame to a wake flame and for complete flame extinction were 55 μm and 75 μm respectively. Future work is also discussed.

I INTRODUCTION

Halon 1301 (CF_3Br) is used principally as a fire suppressant, especially when effective, efficient and clean fire control is needed (Gann, 1995). However, it is one of the chemicals identified to be detrimental to stratospheric ozone. The production of halon 1301 was stopped on January 1, 1994. In order to reduce and eventually eliminate the dependence on halon 1301, researches to find effective

* Corresponding author: E-mail: chchen@cc.nctu.edu.tw. Tel.: 886–3–5712121. Ext. 55130. Fax: 886–3–5721091

replacements have been carried out at the National Institute of Standards and Technology (NIST). Whenever a new replacement has been identified, evaluating its effectiveness in fire suppression becomes a crucial issue. A bench scale apparatus was designed at NIST (Grosshandler *et al.*, 1996A and 1996B) for evaluating the fire suppression efficiencies of new advanced liquid agents. A schematic of this apparatus can be found in Yang *et al.* (1999A and 1999B). It mainly consists of two components: a Tsuji burner (Tsuji and Yamaoka, 1967) and a liquid aerosol delivery system. The motivation of the present work is to understand the interaction between the suspended droplets in the air flow and the counterflow diffusion flame, by extending the previous research results from Chen and Weng (1990) with a water mist included in the combustion model, (see Fig. 1).

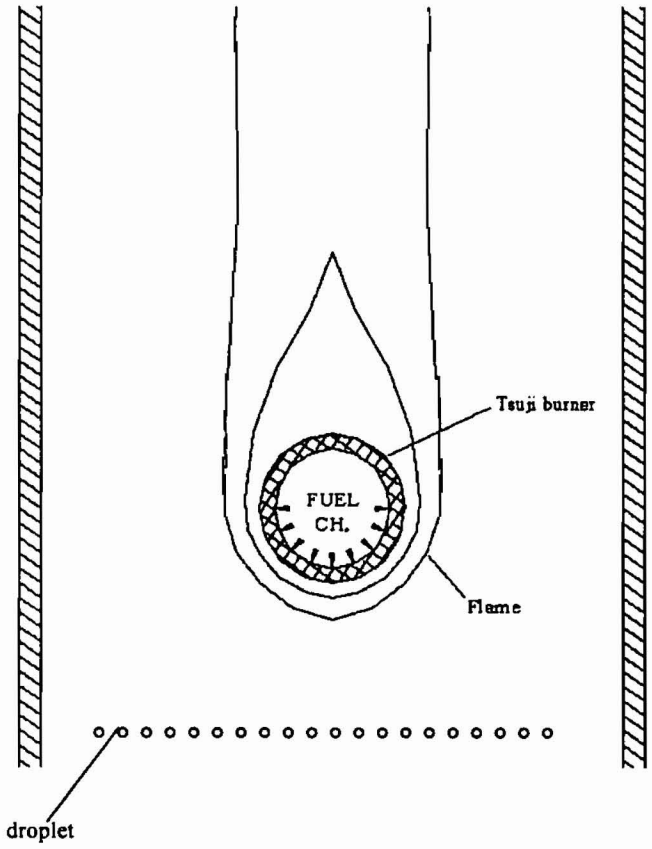

FIGURE 1 Representative figure of the problem

The ability to predict the heat and mass transfer of a cloud of droplets suspended in gas flow is also important in the design of many industrial processes, such as spray dryers, cyclone separators, liquid and solid-fuelled combustion and sprinkler spray systems. In all cases the flow itself consists of a continuous phase, which may be gaseous or liquid, and one or more dispersed phases in the form of solid particles, liquid droplets, or gas bubbles. In general, the motion of the dispersed phase will be influenced by the continuous phase and vice versa. The analysis of multiphase flow is complicated by the need to account for the mass, momentum, and energy coupling between phases. The coupling phenomena, as illustrated in Fig. 2, involves a very complex interaction that affects both the gas and droplet phases.

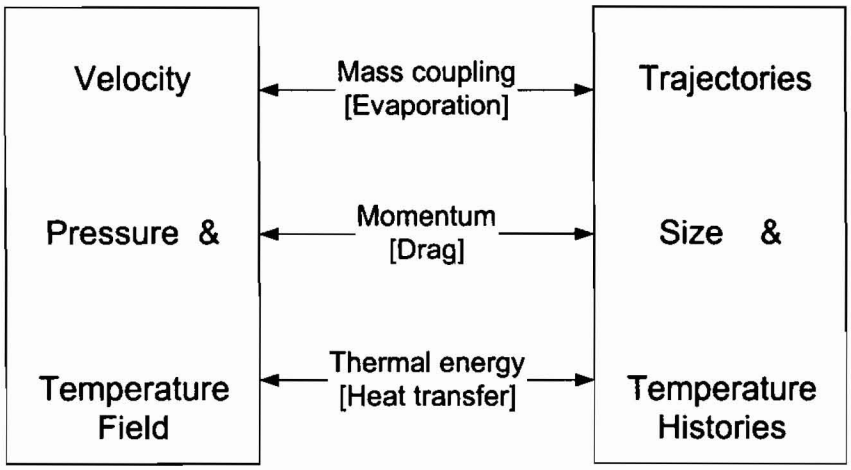

FIGURE 2 Gas-droplet coupling mechanism (Crowe et al., 1977)

Numerous analytical and experimental studies have been made on the aerodynamics of liquid sprays. The review by Faeth (1977) presented a concise summary of spray combustion in rocket engines, gas turbines, Diesel engines, and industrial furnace applications. The behavior of individual droplet is a necessary component of two-phase models, and the work on transient droplet evaporation, ignition, and combustion was presented along with a discussion of the important simplifying assumptions involved with modeling these processes. Sirignano (1983) showed the theoretical developments in problems involving droplet vaporization in a high-temperature environment and spray combustion. Four areas of basic phenomena were discussed in some detail: (i) droplet slip and

internal circulation, (ii) transient heating of droplets, (iii) multicomponent fuel vaporization, and (iv) combustion and vaporization of droplet arrays, groups, and sprays. Various relationships among these phenomena were analyzed as well. Michaelides (1997) presented an intensive review of the transient equation of motion for particles, bubbles, and droplets. Some of the early works on the equation of motion as well as the recent advances were explored. Particular emphasis was placed on the semi-empirical forms of the equation, which are widely used in engineering practice. Chen *et al.* (1992) used detailed models for evaporation and heat, mass, and momentum transfer between the gaseous and liquid phase with detailed gas-phase models for chemistry and molecular transport. Attention was focused on conditions under which droplets can cross the flame many times, and on the influence of the initial number density of the flame structure. Magee and Reitz (1986) studied the extinction of plastic fires by water. Their particular emphases was to determine: (1) the response of the various burning plastics to the external radiant heat flux, (2) the effectiveness of the water in suppressing the fire, and (3) the critical water application rates required for extinction as a function of the radiant flux and type of plastic. Jones and Nolan (1995) examined some of the main themes relating to fire extinguishing research on the use of fine sprays, with the emphasis on the use of fine water sprays or mists rather than on the general use of water sprays. They felt that fine sprays or mists should probably have diameters in the 20–120 μm range. Alpert (1985) numerically examined the simplified axisymmetric problem of a sprinkler spray directly above the center of a constant fire source. The outcome of this interaction determined how sprinkler pressure, flow rate, drop size and spray angle, etc. influenced the degree of water penetration through the fire plume to the burning fuel surface. In order to understand the effects of water sprays on fire intensity with an oil fire, downward-directed sprays to interact with a small-scale opposed gasoline pool fire were experimentally studied in an open environment by Kim *et al.* (1996). Another important part of their study focused on the correlation between droplet size and degree of water penetration through the fire plume, which provided quantitative data for clarifying the essential mechanisms in the extinction of a gasoline fire using water sprays. Later, Kim *et al.* (1997) described an experimental investigation of fire extinction limit and enhancement for gasoline pool fire interacting with water mist. They found that the fire extinction mechanisms in an open environment are the cooling of the fuel rather than the fire plumes. The cooling rate of the fuel depends mainly on the amount of water that reaches the fuel pan through the plume and the flame from the nozzle discharge. The effective water flux is one of the physical parameters that can describe this situation. Liu *et al.* (1993) and Liu (1992) considered a steady, planar, premixed flame generated in a stagnation-point, two-phase flow in which the disperse phase was

simulated by a monodisperse, dilute, and chemically inert spray. Their study focused on a description of the flame extinction under the influences of the Lewis number, flow stretch, and internal heat loss coming from the inert spray. Suh and Atreya (1995) used detailed C_2 chemistry and gas phase radiation to calculate the chemical and physical effects of water vapor on the structure of counterflow diffusion flames. They also measured the temperature profiles to prove their numerical results. Yang *et al.* (1999B) used different types of liquids to investigate the fire suppression efficiency over a Tsuji burner experimentally. They (Yang *et al.*, 1999A) also utilized various inert gases and water to discuss the flame extinction situation over the same burner.

Crowe *et al.* (1977) proposed the Particle-Source-In Cell (PSI-Cell) model to describe the coupling of momentum, heat, and mass transfer between gaseous and droplet phases. This concept of regarding the droplet phase as a source of mass, momentum, and energy to the gaseous phase was described and incorporated into a computational model. A steady two-dimensional spray-cooling problem was analyzed to illustrate the applicability of this model. Papadakis and King (1988A and 1988B) made experimental and theoretical analyses of air temperature and humidity profiles in spray drying. The PSI-Cell model was used to predict the droplet trajectories and velocities, air temperature, humidity and velocity fields, and rates of evaporation of the water droplets in a spray dryer equipped with a pressure atomizer. Chow and Fong (1993) applied the Pressure Implicit with Splitting of Operators (PISO) algorithm and PSI-Cell model to numerically study the interaction between a sprinkler and the fire-induced smoke layer. The smoke in the gas phase was simulated using a field model, whereas the droplet motions from the sprinkler was described by Newton's second law with an air drag and the droplet itself was subjected to convective heat transfer from the smoke layer. However, they just visualized the interaction between the airflow pattern, temperature, and droplet properties without considering the droplet evaporation, fire, and suppression effects. Jicha *et al.* (1994) presented a numerical study of turbulent gas-liquid droplet flow using the Lagrangian approach for the discrete phase and Eulerian approach for the continuous phase. The effects of different directional angles as well as the angle of spray on the velocity and temperature field of the main phase were studied.

This study applied a numerical algorithm to investigate the performance of an evaluation apparatus for halon replacement agents, as described in Yang *et al.* (1999A and 1999B). The main objective is to understand the characteristics and controlling mechanisms of heat and mass transfer between the droplet and flame that may lead to the reduction of flame strength and/or extinction. Since the water mist is suspended in the incoming airflow, the flow field is a liquid-gas two-phase flow. This two-phase flow passes through a two-dimensional, laminar

counterflow diffusion flame established by a Tsuji burner (Tsuji and Yamaoka, 1967), as illustrated in Fig. 1. Using the variations in the droplet size (or mass) and the flow velocity, the maximum concentration of the suppressant as a function of the stretch rate at a fixed fuel ejection velocity can be determined. This process can be used as an evaluation tool for the fire suppression efficiency of new agents by comparing their performance with that of water droplets.

II MATHEMATICAL ANALYSIS

2.1 Gas phase model

In order to make the problem more tractable, several assumptions are made:

1. The flow is steady, two-dimensional, and laminar with Stoke's hypothesis.
2. Radiant heat transfer is neglected.
3. The viscous dissipation and compression work are neglected owing to the low speed combustion problem.
4. The ideal gas law is applicable to the gas mixture with constant and equal specific heats, equal diffusion coefficients and constant Prandtl and Lewis numbers.
5. The average molecular weight is constant.
6. The Soret and Duffour effects, as well as pressure gradient diffusion, are not considered.
7. The temperature on the cylinder surface is constant.
8. Due to the ultra small size/weight of the mists, the gravity force acting on the drops can be neglected.

The gas phase chemistry is described by a one-step overall chemical reaction. Gaseous fuel reacts with oxidizer to form products and releases heat, that is:

$$1\ \text{Kg [Methane]} + \text{f Kg [Oxidizer]} \rightarrow (1+\text{f})\ \text{Kg [Product]} + \text{Q KJ [Heat]} \tag{1}$$

where f and Q represent the stoichiometric oxidizer/fuel mass ratio and the heat of combustion per unit mass of fuel respectively. Therefore, the relationship between mass and energy source terms is:

$$\bar{\dot{\omega}}_{\mathrm{F}} = \bar{\dot{\omega}}_{\mathrm{o}}/\mathrm{f} = -\bar{\dot{\mathrm{Q}}}/\mathrm{Q} \tag{2}$$

The rate equation is assumed to be concentration dependent of second order Arrhenius' law, and the rate equation of fuel becomes:

$$\bar{\dot{\omega}}_{\mathrm{f}} = -\overline{\mathrm{B}}\overline{\rho}^{2}\mathrm{Y}_{\mathrm{f}}\mathrm{Y}_{\mathrm{o}}\exp(-\overline{\mathrm{E}}/\mathrm{R}^{0}\overline{\mathrm{T}}) \tag{3}$$

where $\overline{B}$ and $\overline{E}$ are the frequency factor and the activation energy, respectively.

Since the combustion model is solved nondimensionally, a normalization procedure is given. The nondimensional variables are defined as:

$$x = \frac{\overline{x}}{R},\ y = \frac{\overline{y}}{R},\ u = \frac{\overline{u}}{U_{in}},\ v = \frac{\overline{v}}{U_{in}},\ \rho = \frac{\rho}{\rho^*},\ p = \frac{\overline{P} - \overline{P}_{rc}}{\rho^* U_{in}^2},\ \mu = \frac{\overline{\mu}}{\mu^*},$$
$$Re = \frac{\rho^* U_{in} R}{\mu^*},\ Pr = \frac{\overline{\mu} C_p}{\overline{k}},\ Le = \frac{\overline{k}}{\overline{\rho} C_p \overline{D}},\ T = \frac{\overline{T}}{T^*},\ Q = \frac{\overline{Q}}{C_p T^*},$$
$$E = \frac{\overline{E}}{R^o T^*},\ Da = \frac{R/U_{in}}{1/(\rho^* \overline{B} \exp(-\overline{E}/R^0 T^*))},\ \dot{m} = \frac{\overline{\dot{m}}}{\rho^* U_{in}},$$
$$-f_w = \left(\frac{v_w}{U_{in}}\right)\left(\frac{Re}{2}\right)^{0.5} \tag{4}$$

where U_{in} is the inflow velocity, R the cylinder radius, and T^* the reference temperature, which is arithmetic average of ambient and adiabatic flame temperatures.

Based on the nondimensional variables and parameters just defined, the resultant dimensionless governing equations are presented as follows: Continuity equation:

$$\frac{\partial(\rho u)}{\partial x} + \frac{\partial(\rho v)}{\partial y} = 0 \tag{5}$$

x-momentum equation:

$$\rho u \frac{\partial u}{\partial x} + \rho v \frac{\partial u}{\partial y} =$$
$$-\frac{\partial p}{\partial x} + \frac{\partial}{\partial x}\left\{\frac{\mu}{Re}\left[2\frac{\partial u}{\partial x} - \frac{2}{3}\left(\frac{\partial u}{\partial x} + \frac{\partial v}{\partial y}\right)\right]\right\} + \frac{\partial}{\partial y}\left[\frac{\mu}{Re}\left(\frac{\partial v}{\partial y} + \frac{\partial u}{\partial x}\right)\right] \tag{6}$$

y-momentum equation:

$$\rho u \frac{\partial v}{\partial x} + \rho v \frac{\partial v}{\partial y} =$$
$$-\frac{\partial p}{\partial y} + \frac{\partial}{\partial y}\left\{\frac{\mu}{Re}\left[2\frac{\partial v}{\partial x} - \frac{2}{3}\left(\frac{\partial u}{\partial x} + \frac{\partial v}{\partial y}\right)\right]\right\} + \frac{\partial}{\partial x}\left[\frac{\mu}{Re}\left(\frac{\partial u}{\partial x} + \frac{\partial v}{\partial y}\right)\right] \tag{7}$$

Energy equation:

$$\rho u \frac{\partial T}{\partial x} + \rho v \frac{\partial T}{\partial y} = \frac{1}{Re\ Pr}\left[\frac{\partial}{\partial x}\left(\mu \frac{\partial T}{\partial x}\right) + \frac{\partial}{\partial y}\left(\mu \frac{\partial T}{\partial y}\right)\right] - Q\dot{\omega}_f \tag{8}$$

Fuel species equation:

$$\rho u\frac{\partial Y_f}{\partial x}+\rho v\frac{\partial Y_f}{\partial y}=\frac{1}{\mathrm{Re\ Pr}\ Le}\left[\frac{\partial}{\partial x}\left(\mu\frac{\partial Y_f}{\partial x}\right)+\frac{\partial}{\partial y}\left(\mu\frac{\partial Y_f}{\partial y}\right)\right]+\dot{\omega}_f \tag{9}$$

Oxidizer species equation:

$$\rho u\frac{\partial Y_o}{\partial x}+\rho v\frac{\partial Y_o}{\partial y}=\frac{1}{\mathrm{Re\ Pr}\ Le}\left[\frac{\partial}{\partial x}\left(\mu\frac{\partial Y_o}{\partial x}\right)+\frac{\partial}{\partial y}\left(\mu\frac{\partial Y_o}{\partial y}\right)\right]+f\ \dot{\omega}_F \tag{10}$$

where

$$\dot{\omega}_F=-Da\rho^2 Y_f Y_o\exp(E-E/T) \tag{11}$$

is the nondimensional fuel reaction rate.

The equation of state is,

$$\rho=1/\mathrm{T} \tag{12}$$

and the viscosity variation with temperature is taken to be:

$$\mu=\mathrm{T}^{0.75} \tag{13}$$

The nondimensional boundary conditions are:

At $x = x_{in}$:

$$\mathrm{u}=1,\ \mathrm{v}=0,\ \mathrm{T}=0.24,\ \mathrm{Y_f}=0,\ \mathrm{Y_o}=0.233 \tag{14}$$

At $x=x_{out}$:

$$\frac{\partial \mathrm{u}}{\partial \mathrm{x}}=0,\ \mathrm{v}=0,\ \frac{\partial T}{\partial x}=\frac{\partial Y_f}{\partial x}=\frac{\partial Y_o}{\partial x}=0 \tag{15}$$

At $y=y_{wall}$:

$$\mathrm{u}=\mathrm{v}=0,\ \frac{\partial T}{\partial y}=\frac{\partial Y_f}{\partial y}=\frac{\partial Y_o}{\partial y}=0 \tag{16}$$

At $y=0$:

$$\frac{\partial \mathrm{u}}{\partial \mathrm{y}}=0,\ \mathrm{v}=0,\ \frac{\partial T}{\partial y}=\frac{\partial Y_f}{\partial y}=\frac{\partial Y_o}{\partial y}=0 \tag{17}$$

At $-1<x\le 0,\ \sqrt{x^2+y^2}=1$:

$$\mathrm{v_t}=0,\ \mathrm{v_n}=-\mathrm{f_w}(2/\mathrm{Re})^{0.5},\ \mathrm{T_w}=0.32,\ \dot{\mathrm{m}}_\mathrm{w}=\mathrm{v_n}\rho_\mathrm{w}$$

$$\dot{\mathrm{m}}_\mathrm{w}\ \mathrm{Y_{fw}}=\dot{\mathrm{m}}_\mathrm{w}+\frac{1}{\mathrm{Re\ Pr\ Le}}\mu\frac{\partial \mathrm{Y_f}}{\partial \mathrm{n}}|_\mathrm{w}$$

$$\dot{\mathrm{m}}_\mathrm{w}\ \mathrm{Y_{ow}}=\frac{1}{\mathrm{Re\ Pr\ Le}}\mu\frac{\partial \mathrm{Y_o}}{\partial \mathrm{n}}|_\mathrm{w} \tag{18}$$

At $0\le x\le 1,\ \sqrt{x^2+y^2}=1$:

$$v_t = 0,\ v_n = 0,\ T_w = 0.32,\ \dot{m}_w = 0$$
$$\frac{\partial Y_f}{\partial n}|_w = 0,\ \frac{\partial Y_o}{\partial n}|_w = 0 \tag{19}$$

Note that the nondimensional ejecting velocity of the fuel, $-f_w$, from the cylinder is adopted from the experimental data by Tsuji.

2.2 Droplet model

In order to evaluate the source terms in the gas-phase reacting flow equations due to the presence of droplets, it was necessary to establish the droplet trajectories, sizes, and temperature histories. In other words, a set of equations was required to describe the droplet momentum, heat transfer, and mass diffusion. This was accomplished by integrating the droplet equation of motion and the heat and mass transfer equations related to droplet temperature and size. In turn, the velocity, pressure, and temperature fields in the gas phase were used in these calculations. The coupling mechanism is illustrated in Fig. 2.

According to Crowe et al. (1977), the following assumptions were made to further simplify this model: (a) Water droplets were assumed to be spherical without rotation. (b) Infinite conductivity in the droplet phase, i.e. the droplets had a uniform temperature at any instant. (c) No droplet-to-droplet interaction was considered so that there were no collisions between droplets and droplet breaking-up. (d) The radiation on the droplets was not taken into account. (e) Droplet deformation caused by surface shear force was neglected. (f) The other terms contributing to the aerodynamic forces on the droplet, namely the pressure gradient, virtual mass and Basset term, were neglected because they were of the order of the gas/droplet density ratio, which for most applications are approximately 10^{-3}. (g) The Saffman lift and Magnus forces were also neglected because the droplets were not in a high-shear region of the gas flow. (h) Due to the ultra light mists, the gravitational acceleration of liquid droplets is expected to be very small. Thus, it is not under consideration in equation (20).

With the above assumptions and according to Newton's second law with an air drag, the equation of motion for a droplet is given by:

$$\frac{d\vec{V}}{dt} = \left(\frac{18\mu}{\rho_d d^2} \times \frac{C_D \mathrm{Re}_d}{24}\right)(\vec{U} - \vec{V}), \tag{20}$$

The Reynolds number, based on the gas-droplet relative velocity, is:

$$\mathrm{Re_d} = \rho \frac{\left|\vec{\mathrm{U}} - \vec{\mathrm{V}}\right| \mathrm{d}}{\mu}, \tag{21}$$

For a non-evaporating droplet, the drag coefficient can be represented by Wallis (1969):

$$C_{D_0} = \frac{24}{\mathrm{Re}_d}(1 + 0.15\ \mathrm{Re}_d{}^{0.687}) \tag{22}$$

The rate of decrease in droplet mass is given by:

$$\frac{\mathrm{dm_d}}{\mathrm{dt}} = -\mathrm{Sh}(\rho \mathrm{D})\pi \mathrm{d}(\mathrm{Y} - \mathrm{Y}_\infty), \tag{23}$$

where Sh is the Sherwood number, calculated from:

$$\mathrm{Sh} = 2 + 0.6\ \mathrm{Re_d}{}^{0.5}\mathrm{Sc}^{0.33};\ \mathrm{Sc} = \frac{\mu}{\rho \mathrm{D}}. \tag{24}$$

Using the above equation, the decreasing rate in droplet diameter with time can be written as:

$$\frac{\mathrm{d(d)}}{\mathrm{dt}} = -2\mathrm{Sh}(\rho \mathrm{D})\frac{\mathrm{Y} - \mathrm{Y}_\infty}{\rho_\mathrm{d}\mathrm{d}}. \tag{25}$$

The heat balance equation for a droplet is:

$$\mathrm{m_d c_d}\frac{\mathrm{dT_d}}{\mathrm{dt}} = \dot{\mathrm{q}} + \mathrm{h_{fg}}\frac{\mathrm{dm_d}}{\mathrm{dt}}, \tag{26}$$

where $\dot{q}$ is the heat transfer rate to a droplet, h_{fg} the latent heat of vaporization, and c_d the specific heat of a droplet.

The rate of heat transfer to the droplet is obtained from:

$$\dot{\mathrm{q}} = \mathrm{Nu}\pi \mathrm{kd}(\mathrm{T_g} - \mathrm{T_d}), \tag{27}$$

where k is the thermal conductivity of the gas and Nu is the Nusselt number, which varies with the Reynolds number and Prandtl number as Bird *et al.* (1960):

$$\mathrm{Nu} = 2 + 0.6\ \mathrm{Re_d}{}^{0.5}\ \mathrm{Pr}^{0.33};\ \mathrm{Pr} = \frac{\mu}{\rho\alpha} \tag{28}$$

The droplet equations were solved simultaneously with the airflow equations. The fourth-order Runge-Kutta technique was used for the system of ordinary differential equations under different sets of initial conditions. The time interval was kept sufficiently small in order to obtain accurate results.

2.3 Gas-Droplet Computational Procedure

The complete solution procedure for a gas-droplet flow field was executed as illustrated in Fig. 3. Solving the gas flow field assuming no droplets are present begins the calculation. Using this flow field, droplet trajectories together with size and temperature histories along the trajectories were calculated. The mass, momentum, and energy source terms for each cell throughout the flow field were

then determined. The gas flow field was solved again, incorporating these source terms. The new gas flow field was used to establish new droplet trajectories and temperature histories, which constitute the effect of the droplet cloud on the gas phase, thereby completing the cycle of mutual interaction or "two-way" coupling. After several iterations, the flow field equations were satisfied to within a predetermined value, and the solution that accounts for the mutual interaction of the droplets and gas was obtained.

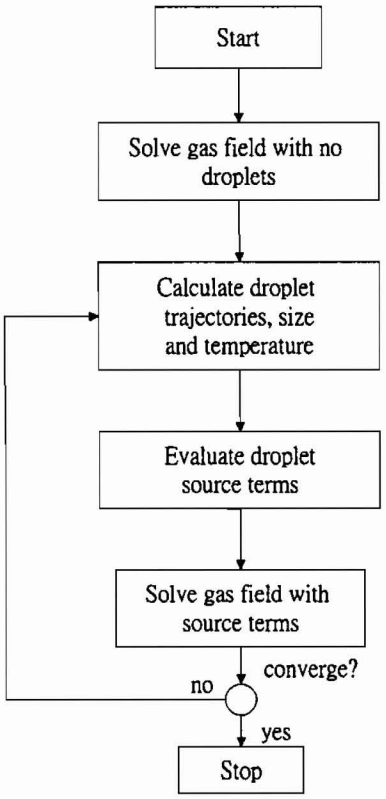

FIGURE 3 Flow chart for PSI-CELL computational scheme (Crowe et al., 1977)

III RESULTS AND DISCUSSION

The dimensionless domain of computation was chosen as $x_{in} = -7$, $x_{out} = 13$, and $y_{wall} = 4$. The corresponding thermodynamic, transport, and chemical kinetic

properties are listed in Table I. After a normalization procedure throughout the model, the non-dimensional parameters appeared are illustrated in Table II.

TABLE I Property values in gas phase

Name	*Symbol*	*Value*	*Units*
Ambient Temperature	$\overline{T}_a$	300	K
Reference Temperature	T^*	1250	K
Density (reference)	ρ^*	0.2835	Kg/m^3
Viscosity (reference)	ν^*	1.69×10^{-4}	m^2/s
Thermal Diffusivity (reference)	α^*	2.36×10^{-4}	m^2/s
Specific Heat	C_p	1.351	KJ/Kg K
Frequency Factor	$\overline{B}$	1.58×10^9	m^3/Kg s
Activation Energy	$\overline{E}$	1.35×10^5	KJ/Kg-mole
Heat of Reaction	$\overline{Q}$	4.95×10^4	KJ/Kg-fuel
Cylinder surface temperature	$\overline{T_w}$	400	K
Oxidizer velocity	U_{in}	0.75	m/s
Fuel-ejecting velocity	v_w	0.1221	m/s
Cylinder radius	R	0.015	m

TABLE II Non-dimensional Parameters

Symbol	*Definition*	*Value*
Re	$U_{in}R/\nu^*$	66.6
Pr	$\overline{\nu}/\overline{k}$	0.73
Le	$\overline{\alpha}/\overline{D}$	0.833
T_w	$\overline{T}_w/T^*$	0.32
Y_{oa}	–	0.231
f	–	4.0
Q	$\overline{Q}/C_pT^*$	29.28
E	$\overline{E}/R^0T^*$	13.0
Da	$(R/U_{in})\rho^*\overline{B}\exp(-\overline{E}/R^0T^*)$	20
$-f_w$	$(v_w/U_{in})(Re/2)^{0.5}$	0.5

3.1 The Effects of Varying Water Vapor Mass Fraction in Air

The first step was to consider the effects of varying water vapor mass fraction (Y_{H_2Oa}) in the inflow air without the presence of droplets on the flame behavior. As listed in Table III, the vapor mass fraction varied from 0 to 0.19 whereas the Damkohler number (Da), flame stretch rate ($2U_{in}/R$), and fuel ejection velocity (f_w) were fixed with values of 20, 100 and 0.5, respectively. Note that case A1 is designated as the reference case under the conditions just mentioned without water vapor in the incoming flow.

TABLE III Effect of varying vapor fraction

Case	*Vapor fraction* $Y_{H_2O\infty}$	*mass Flame type*
B1	0.	Envelope
B2	0.1	Envelope
B3	0.18	Envelope
B4	0.19	Blowoff

Da-20 2Uin/R=100 and fw=0.5 for all cases

The resultant isotherm distributions over the Tsuji burner as a function of Y_{H_2Oa} are displayed in Fig. 4. Case B1 is exactly the same as case A1, in which burning occurs in dry air. As Y_{H_2Oa} increases up to 0.18, the envelope flame can still be retained. However, the flame zone becomes thinner and smaller; see the variation in the temperature contour T = 1750K. This is not caused by the flame stretch effect since the inlet flow velocity is maintained at a constant for these cases. After that, a slight increment in Y_{H_2Oa} from 0.18 (case B3) to 0.19 (case B4), the flame is diminished abruptly in the flow field. Between the envelope flame and extinction, no side or wake flames are found. This phenomenon is quite different from that shown in the previous study by Chen and Weng (1990). It can be explained as follows. When the ambient vapor fraction increases, the ambient oxidizer mass fraction is decreased relatively, indicating that the oxygen concentration in the flow field is diluted. From the expression of gas phase chemical kinetics, the chemical reaction rate is slowed down to reduce the heat release rate. In other words, the flame becomes weaker and weaker as the oxygen concentration is lowered. As soon as the limit (Y_{Oa} = 0.189 in this study) is reached, the reaction can no longer be sustained and extinction occurs instantaneously. The effect of varying the water vapor mass fraction in the inflow air can be regarded as discharging inert gases, such as CO_2, into the burning item to extinguish the fire.

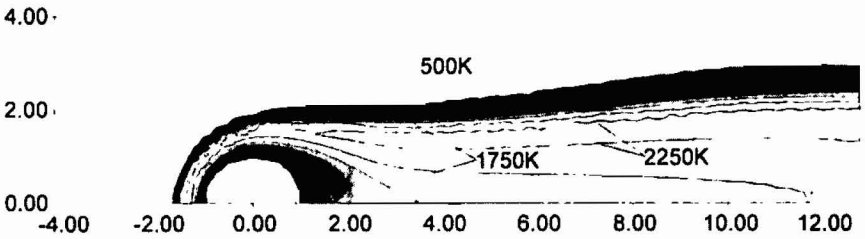

(B1) $Y_{H_2O_a}=0$ ($Y_{OA}=0.233$)

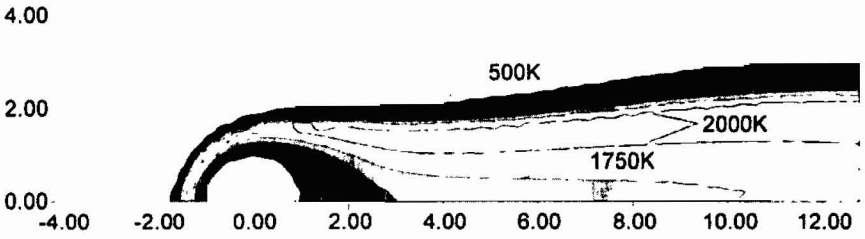

(B2) $Y_{H_2O_a}$ =0.10($Y_{OA}=0.210$)

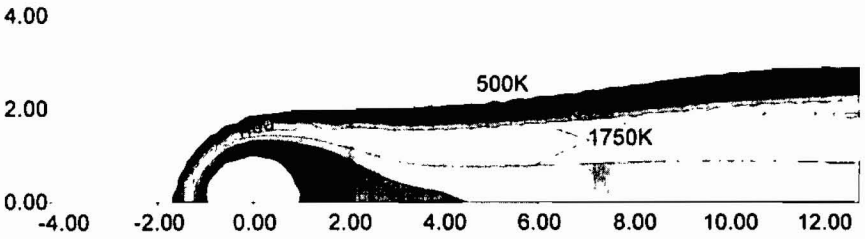

(B3) $Y_{H_2O_a}$ =0.18($Y_{OA}=0.191$)

FIGURE 4 Series of temperature contour distributions for changing ambient vapor fraction

3.2 The Effects of Varying the Mist Flow Rate on the Envelope Flame

Since the main objective of this study was to evaluate the fire suppression efficiencies of water mist over a diffusion flame generated by a Tsuji burner, a parametric study, based on the change in droplet size, is given. Two initial droplet sizes, 50 μm and 80 μm, were used. For each droplet size, several mist flow rates, were selected. The mist flow rates, defined as ((the volume flow rate of

inlet droplets)/(the volume flow rate of inflow air))•100%, are listed in Tables IV and V. If the droplet size is fixed, then, the number flow rate, defined as the number of droplets passing through the port per unit time, is proportional to the mist flow rate. The droplets distribute uniformly at the inlet ports, and their velocities and temperatures are the same as the inlet free stream. Numerically, the water mists are equally separated into ten specified positions in the half plane at $x = x_{in}$, which are y=0.2, 0.6, 1.0, 1.4, 1.8, 2.2, 2.6, 3.0, 3.4 and 3.8. Also at the inlet, the droplet sizes are the same, i.e., the monodisperse model is assumed.

TABLE IV Effect of mist flow rate for 50 μm droplets

Case	*Mist flow rate*	*Flame type*
C1	5%	Envelope
C2	6%	Envelope
C3	7%	Wake
C4	15%	Wake
C5	16%	Blowoff

Da-20 $2U_{in}/R = 100$ and $f_w = 0.5$ for all cases

TABLE V Effect of mist flow rate for 80 μm droplets

Case	*Mist flow rate*	*Flame type*
D1	3%	Envelope
D2	4%	Envelope
D3	4.5%	Wake
D4	5%	Wake
D5	10%	Wake
D6	11%	Blowoff

Da-20 $2U_{in}/R = 100$ and $f_w = 0.5$ for all cases

In the simulation, the burning conditions of an envelope flame subjected to Da = 20 and $f_w = 0.5$ in a dry airflow field (case A1 or B1) were chosen. The corresponding temperature and vapor mass fraction distributions are shown in Fig. 5, which serves as the base case. The temperature distribution was discussed previously. The H_2O vapor distribution, illustrated in Fig. 5(b), was generated only by the chemical reaction. Its profile is therefore similar to the temperature profile.

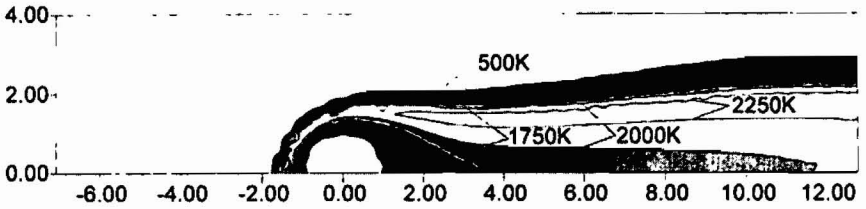

FIGURE 5(a) Temperature contour distribution (case A1)

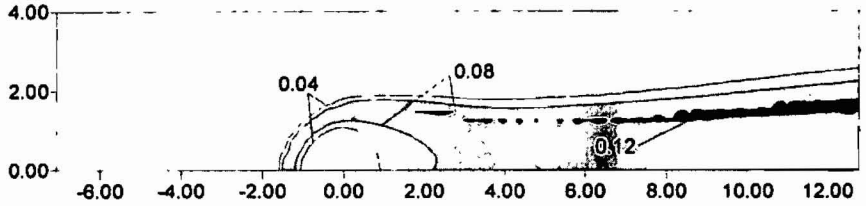

FIGURE 5(b) Water vapor fraction contoukjr (case A1)

3.2.1 50 μm Droplets

Figure 6 shows the temperature and H_2O vapor mass fraction distributions as well as the droplet trajectories for the 50 μm droplet under a 5% mist flow rate. It can be seen that the envelope flame is still surrounding the porous section of the cylinder. However, compared to the flame in Fig. 5 (case A1), the flame temperature is lower and the flame thickness ahead of the cylinder is thinner; see T = 2000K's contour line for an example. This indicates that the flame is weaker. Since the incoming flow velocity and blowing velocity are the same as case A1, the reduction of flame strength in this case is apparently caused by the presence of mist. Comparing Fig. 6(b) with 5(b), the presence of mist does alter the combustion features greatly.

In order to understand the contribution from the droplet vaporization process, Figure 6(c) shows the trajectories of the ten droplets in the flow field. The fluid moves from left to right. Note that the endpoint of each trajectory is the location where the specified droplet is fully vaporized, i.e., no liquid phase exists after that point. It can be seen that no droplet can penetrate into the flame and all of them disappear on the outside of the flame. No liquid droplet exists downstream of x = 6 in this case. The two droplets near the symmetric line, y = 0, are completely vaporized ahead of the cylinder. These two droplets are subjected to the

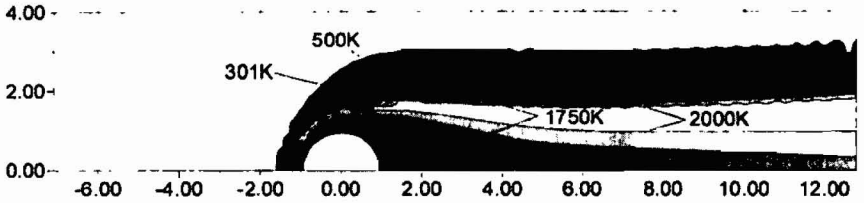

FIGURE 6(a) Temperature contour distribution (case C1)

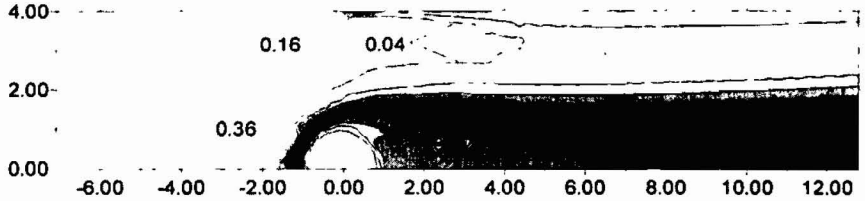

FIGURE 6(b) Water vapor fraction contour (case C1)

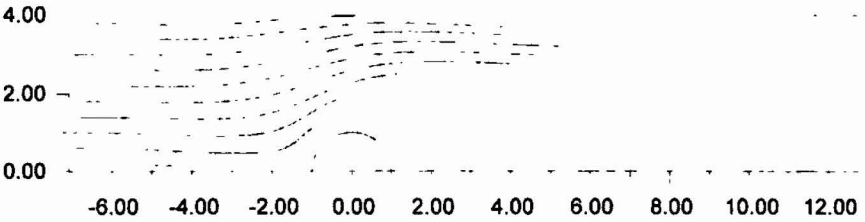

FIGURE 6(c) Droplet trajectories (case C1)

strongest adverse pressure and heat flux from the flame front, consequently, their velocities are retarded substantially, and they are quickly vaporized. The other droplets are deflected outward as they approach the flame due to the high-pressure plateau generated inside the flame and the blowing from the forward part of the cylinder. The deflection is suppressed near the upper wall. Because the vapor concentration near the wall is less than other places in the flow field, the concentration gradient is very steep near the wall. The droplets near the upper wall are vaporized completely at a shorter distance with respect to the other droplets. Droplets away from the wall and symmetric line can travel further downstream.

In Fig. 6(b), the vapor distribution ahead of the cylinder extends upstream, indicating that the droplets near the symmetric line, y = 0, have been vaporized intensively. Near the upper wall, vapors are generated by droplets due to the concentration gradient effect as mentioned in the previous paragraph. Since all the droplets are vaporized outside the flame, the vapor is carried downstream by convection. The vapor mass fraction in Fig. 6(b) is much higher than that in Fig. 5(b) in the downstream flame and plume regions because it is comprised of vapor generated from the reaction zone and vapor convected from upstream due to droplet vaporization.

To summarize, each droplet traveling along its own trajectory is subjected to heat flux from the flame. Subsequently, the droplet temperature rises such that the evaporation becomes intense and generates more vapors in the gas phase. During this process, the flame loses heat and the vapor transformed from the liquid droplets dilute the oxidizer and fuel concentrations. Both effects contribute to the lowering of the flame strength.

Figure 7 shows the temperature and H_2O vapor mass fraction distributions as well as the droplet trajectories for the 50 μm droplet size under a 6% mist flow rate. The increase of mist flow rate results in an increase of the number flow rate. The combustion features are similar to that in Fig. 6. The flame strength is weakened further since it is subjected to more coolant. Compared to the last case (5% mist flow rate), the droplets near the stagnation line can move closer to the flame, indicating that the flame becomes weaker. For 50 μm droplets, the 6% mist flow rate is the upper limit for the existence of an envelope flame.

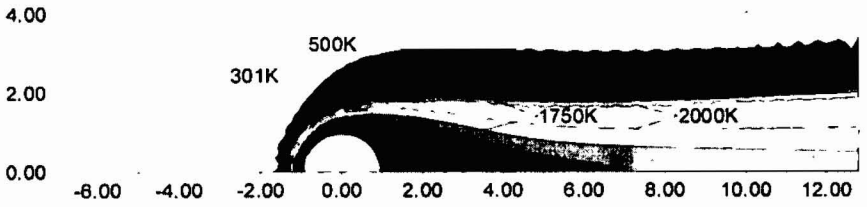

FIGURE 7(a) Temperature contour distribution (case C2)

Figure 8(a) shows that as the mist flow rate increases to 7%, the flame front is extinguished ahead of the cylinder, and it retreats downstream becoming a wake flame. As shown in Fig. 8(c), the droplet near the symmetric line now can slip over the cylinder surface but does not impinge on it due to the blowing. However, most of the droplets, including the one near the upper wall, disappear between x = 3 and x = 4. The two droplets that are closest to the flame front vaporize much earlier.

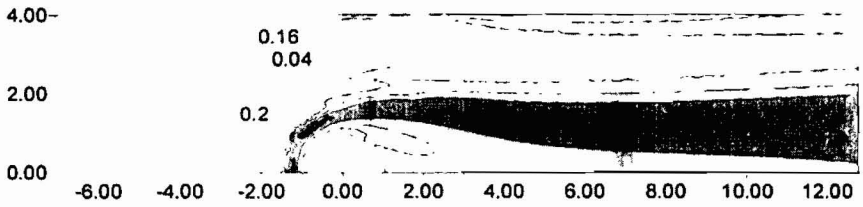

FIGURE 7(b) Water vapor fraction contour (case C2)

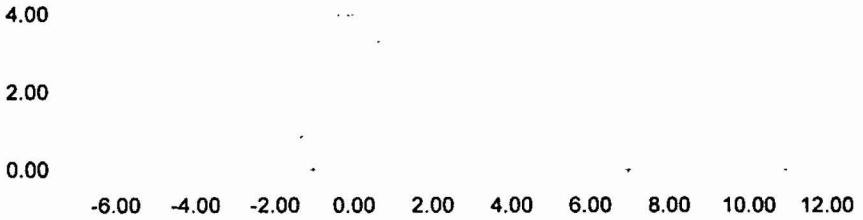

FIGURE 7(c) Droplet trajectories (case C2)

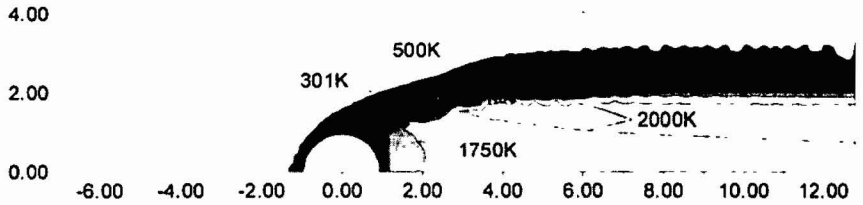

FIGURE 8(a) Temperature contour distribution (case C3).

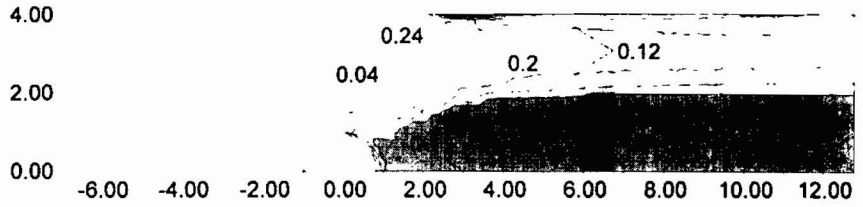

FIGURE 8(b) Water vapor fraction contour (case C3)

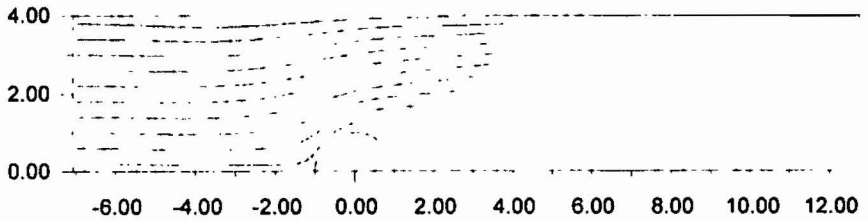

FIGURE 8(c) Droplet trajectories (case C3)

As illustrated in Fig. 9(a), the wake flame can survive up to 15% of the mist flow rate, above which no flame exists in the flow field and extinction occurs. Comparing with Fig. 8(a), the flame is much weaker as expected. The droplets are therefore able to travel a little further downstream. Considering the magnitude of the increment in mist flow rate, the change in flame seems not too substantial. This may be due to the fact that the flame front hides behind the cylinder and is not directly subjected to droplet impingement. The vapor generated outside the flame is transported into the flame by diffusion, but not by convection. The wake flame can therefore survive longer than the envelope flame.

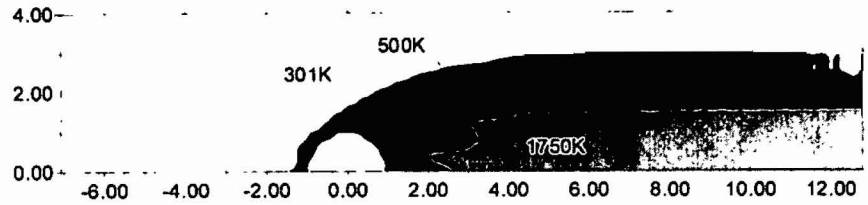

FIGURE 9(a) Temperature contour distribution (case C4)

3.2.2 80 μm Droplets

For the 80 μm droplet, the resultant flame is a wake flame at 5% mist flow rate. A series of computations for lower mist flow rates were performed. Fig. 10 shows the temperature and H_2O vapor mass fraction distributions as well as the droplet trajectories under a 3% mist flow rate. They are quite similar to those in Fig. 6.

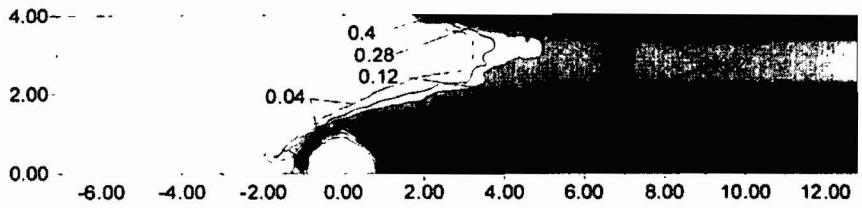

FIGURE 9(b) Water vapor fraction contour (case C4)

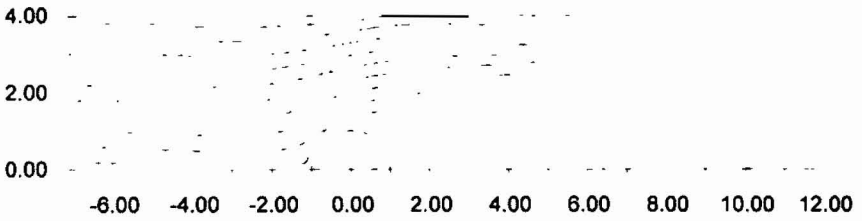

FIGURE 9(c) Droplet trajectories (case C4)

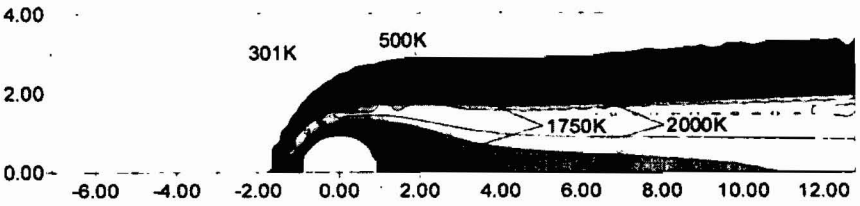

FIGURE 10(a) Temperature contour distribution (case D1)

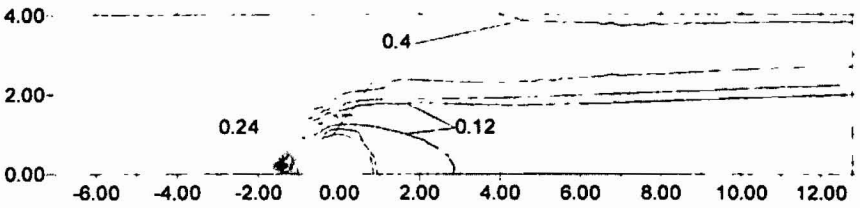

FIGURE 10(b) Water vapor fraction contour (case D1)

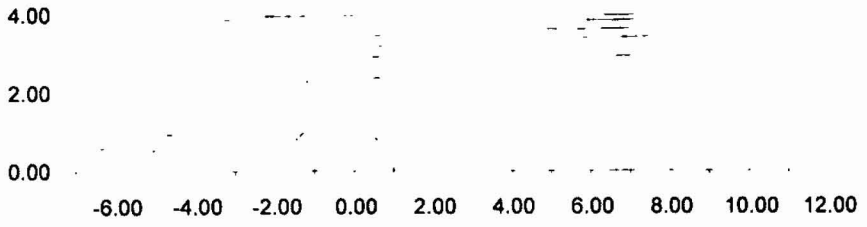

FIGURE 10(c) Droplet trajectories (case D1)

At a one percent increase in the mist flow rate, the flame shown in Fig. 11(a) is somewhat different from the one in Fig. 10(a). The flame front now is shifted outward slightly from the symmetric line, in other words, it no longer completely covers the cylinder. The vapor can therefore penetrate into the front stagnation region which results in a high local mass fraction of H_2O (Y_{H_2O}= 0.6); see Fig. 11(b). The vapor mass fraction in the flame front is about 0.28, which is close to the corresponding mass fraction (Y_{H_2O}= 0.24) in the last case that the flame fully encloses the cylinder. The two droplets near the symmetric line effectively attack the flame front. It can be seen from Fig. 11(c) that the two droplets have enough momentum to flow up to the front part of the cylinder and vaporize quickly and completely. As a consequence, the H_2O vapors causes a high H_2O vapor mass fraction in the stagnation region, shown in Fig. 11(b), which reduces the oxidizer and fuel concentrations to slow down the local reaction. The flame loses heat by the heat absorption for droplet evaporation.

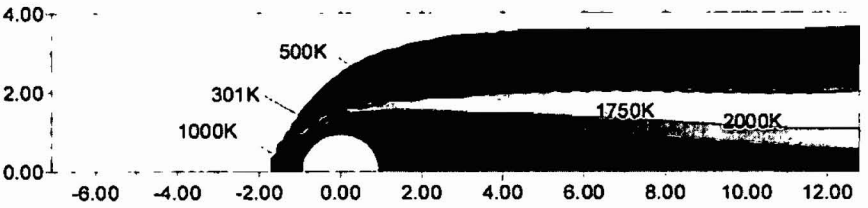

FIGURE 11(a) Temperature contour distribution (case D2)

Since the flame front in the last case (4% mist flow rate) is weak, a little increase in the mist flow rate to 4.5% leads to a wake flame as shown in Fig. 12(a). The wake flame is retained up to the 10% mist flow rate (Fig. 14). Above that critical value, no flame is found in the flow field.

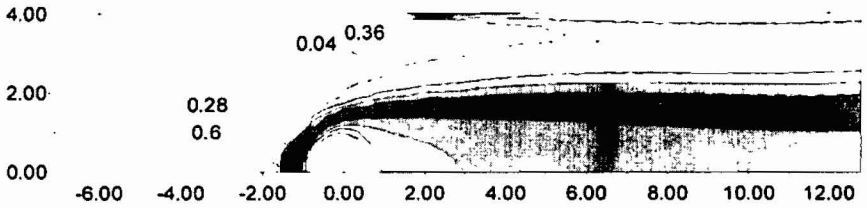

FIGURE 11(b) Water vapor fraction contour (case D2)

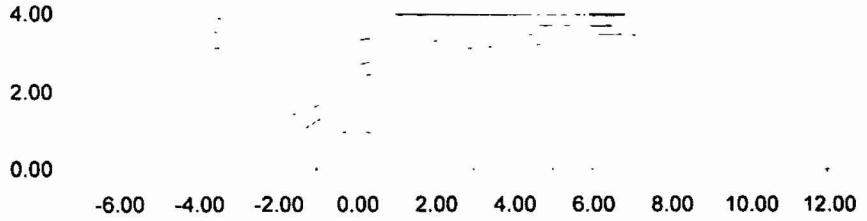

FIGURE 11(c) Droplet trajectories (case D2)

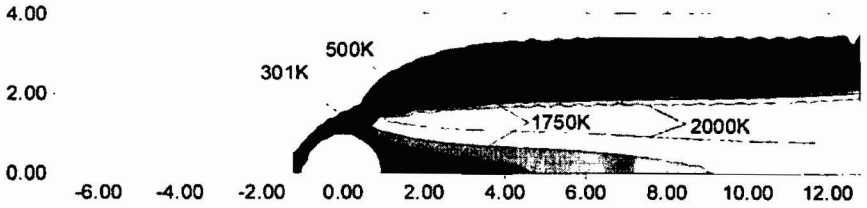

FIGURE 12(a) Temperature contour distribution (case D3)

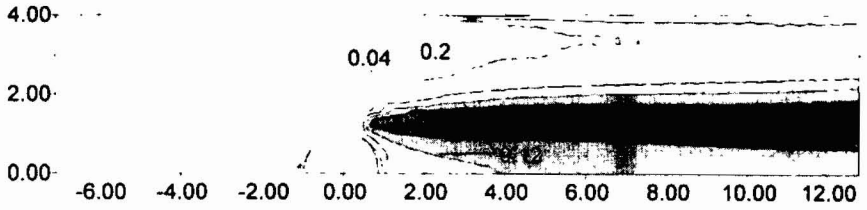

FIGURE 12(b) Water vapor fraction contour (case D3)

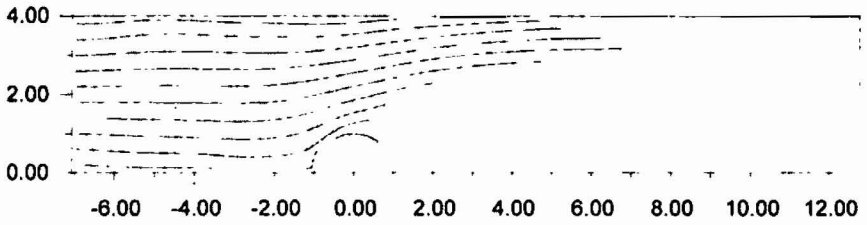

FIGURE 12(c) Droplet trajectories (case D3)

By comparing Fig 6 with Fig. 13, it can be seen that under the same mist flow rate, the larger size of droplet can be more effectively to attack the counter-flow diffusion flame, because the larger droplets have greater inertia that allows greater penetration into the flame or travel further downstream. As the droplets impinge upon the flame, they are vaporized quickly since in the present study the droplet size, even for 80 μm, is still quite small. This vaporization is a heat absorption process that leads to the weakening of the flame. In the meantime, the vapor generated from the droplet evaporation dilute both the oxidizer and fuel concentrations, which further reduces the flame strength.

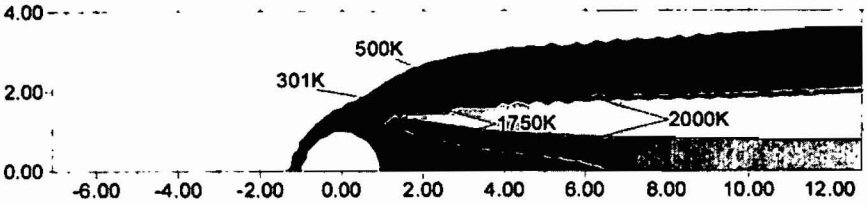

FIGURE 13(a) Temperature contour distribution (case D4)

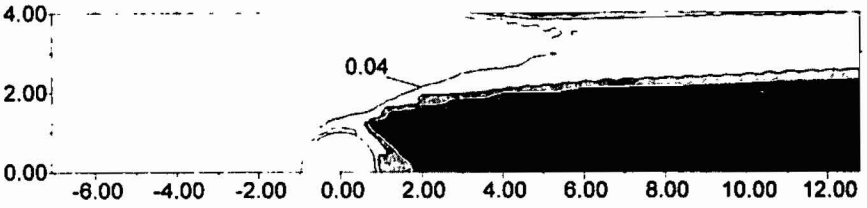

FIGURE 13(b) Water vapor fraction contour (case D4)

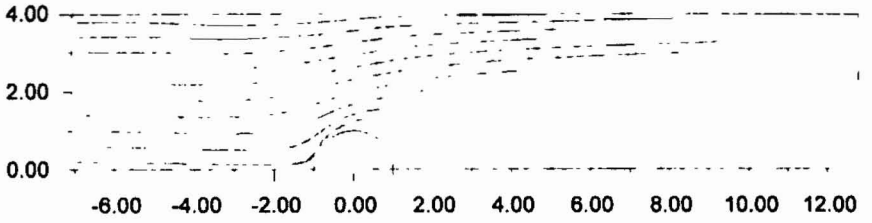

FIGURE 13(c) Droplet trajectories (case D4)

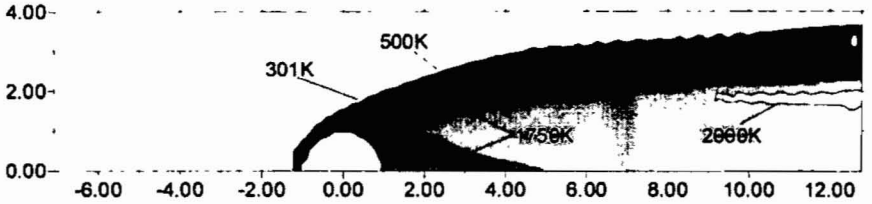

FIGURE 14(a) Temperature contour distribution (case D5)

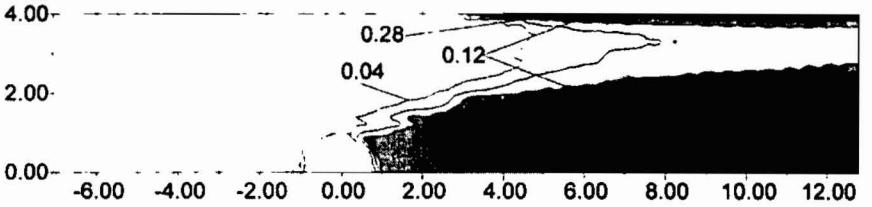

FIGURE 14(b) Water vapor fraction contour (case D5)

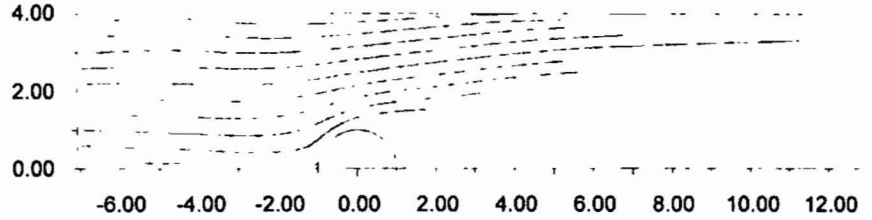

FIGURE 14(c) Droplet trajectories (case D5)

3.3 The Effect of Varying the Droplet Size

In this section, the main objective is to evaluate the fire suppression efficiencies of water mist by changing the droplet size with the same droplet number flow rate. From the number flow rate definition, the mist flow rate will increase with the droplet size as the number flow rate is kept constant. The Damkohler number (Da), flame stretch rate ($2U_{in}/R$), and ejection velocity (f_w) are fixed at values of 20, 100, and 0.5, respectively. In this case study, 50 μm droplets at 5% mist flow rate were adopted as the reference (Fig. 6). The inlet conditions for the droplets, such as distribution, velocities, and temperatures, were the same as that in the previous study. The values of the droplet sizes and the corresponding mist flow rates are listed in Table VI.

TABLE VI Effect of varying droplet size

Case	*Droplet size*	*Mist flow rate*	*Flame type*
E1	50 μm	5%	Envelope
E2	55 μm	6.655%	Wake
E3	60 μm	8.64%	Wake
E4	65 μm	10.985%	Wake
E5	70 μm	13.72%	Wake
E6	75 μm	16.875%	Blow off

Da-20 $2U_{in}/R = 100$ and $f_w = 0.5$ for all cases

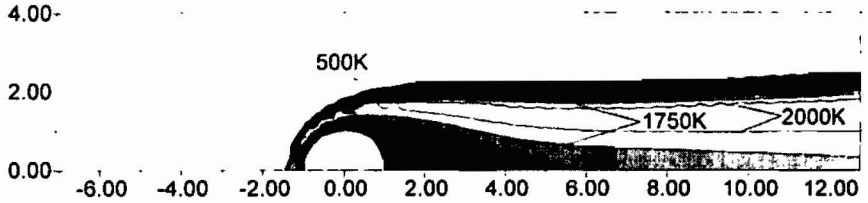

FIGURE 15(a) Temperature contour distribution (case E1)

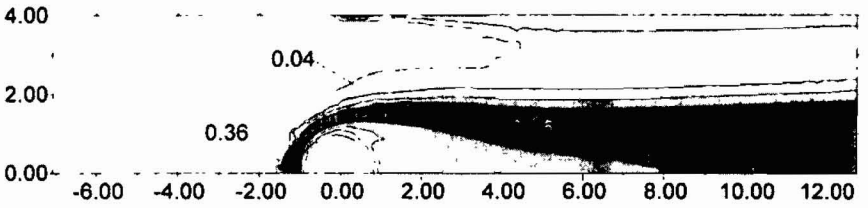

FIGURE 15(b) Water vapor fraction contour (case E1)

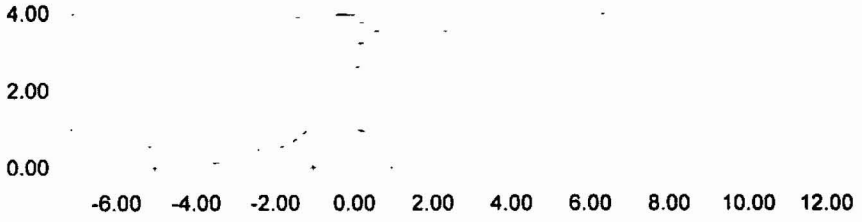

FIGURE 15(c) Droplet trajectories (case E1)

As the droplet size increases up to 55 μm, at which the mist flow rate is 6.655%, as shown in Fig. 16(a), the flame front is extinguished from the area ahead of the cylinder, and it retreats downstream to become a wake flame. From Section 3.1, the envelope flame becomes a wake flame when the mist flow rate is between 6% and 7% for the 50 μm droplets. It is expected that droplets with larger sizes should be more effective in attacking the counter-flow diffusion flame. Therefore, the envelope flame extinction from the front stagnation area under 55 μm droplets at 6.655% mist flow rate is a reasonable solution compared to that in the previous study. The wake flame becomes weaker and weaker with increasing droplet size. As the droplet size is increased up to 70 μm, the wake flame is extinguished from the flow field.

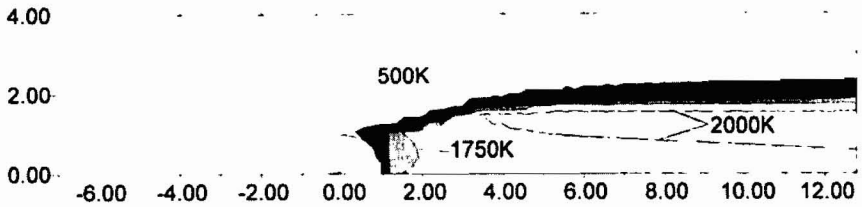

FIGURE 16(a) Temperature contour distribution (case E2)

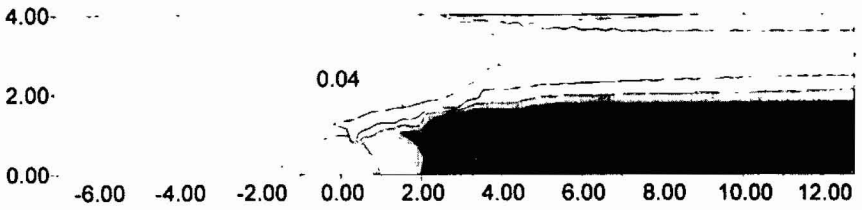

FIGURE 16(b) Water vapor fraction contour (case E2)

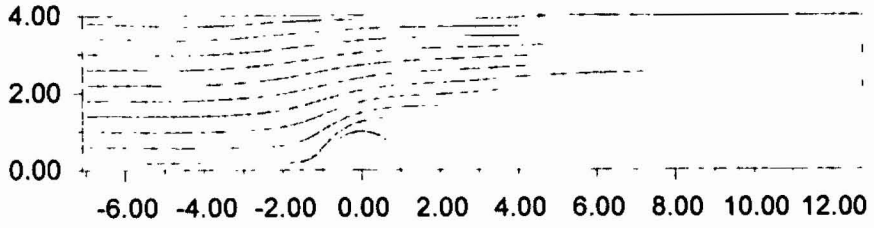

FIGURE 16(c) Droplet trajectories (case E2)

IV CONCLUSION

The flame stabilization and extinction phenomena over a Tsuji burner subjected to a water mist suspended in the incoming airflow was numerically studied. The configuration is similar to the bench scale apparatus developed at NIST for evaluating the fire suppression efficiencies of new advanced liquid agents for halon replacements. This model comprised Eulerian and Lagrangian formulations to describe the two-phase gas-droplet flow and the coupling mechanisms of mass, momentum, and energy between the phases. The gas phase combustion model adopted the one developed by Chen and Weng (1990), which solved the two-dimensional momentum, energy, species, and continuity equations. A one-step overall chemical reaction with a second-order Arrhenius type kinetics was used. The liquid droplet model included dynamic as well as heat and mass transfer equations with some empirical correlations. The two-phase coupling was managed using the PSI-Cell model.

Three parametric studies were carried out in this study. Varying the vapor mass fraction in the inlet air stream without considering the liquid droplet evaporation effect was used in the first study. The second study considered two droplet sizes (50 and 80 μm, respectively) under several mist flow rates. Finally, the effects of droplet size with constant number flow rate were studied. In all cases, the flames were specified with a fixed Damkohler number (or the inlet velocity, implicitly), Da = 20, and fuel-ejection rate, f_w= 0.5.

In the first parametric study, the flame strength was decreased with increasing the vapor mass fraction in the inlet stream. When Y_{H_2Oa} was less than 0.18, an envelope flame existed. As Y_{H_2Oa} increased above the critical value, $Y_{H_2Oa} = 0.18$, the flame was completely diminished in the flow field. No side or wake flame existed. This was due to the dilution of the oxygen concentration caused by the increase in the vapor mass fraction, resulting in a slow chemical reaction. When the critical value was reached, the flame disappeared abruptly.

For the specified size of droplets distributed uniformly in the inlet airflow, the flame size becomes smaller, and the flame temperature becomes lower as a result of increasing mist flow rate. The H_2O vapor mass fractions are increased in the forward stagnation area of the porous burner, the wake region, and the region near the upper wall. While a droplet travels along its trajectory, it is subjected to a large amount of heat from the flame to raise its temperature to enhance evaporation. The substantial change in density from liquid droplet to vapor effectively dilutes the oxygen and fuel concentrations. The flame loses a great amount of heat from the droplet evaporation process. As a consequence, the reaction rate in the flame is reduced substantially in the presence of a water mist. When the mist flow rate is above a certain critical value, 7% for 50 μm droplet size and 4.5 % for 80 μm, the envelope flame retreats downstream of the cylinder and becomes a wake flame. It shows that increasing the mist flow rate at the same inflow velocity condition can lead to a regression of the envelope flame, and it will become a wake flame, eventually. This phenomenon is consistent with the experimental observation by Yang et al. (1999C) that indicates the larger the liquid application rate, the smaller the blow-off velocity. The liquid application rate mentioned in the last reference is equivalent to the droplets volume flow rate, and the blow-off velocity is the critical inflow velocity, which causes the envelope flame to transform into a wake flame. Flame extinction occurs in the flow field as the mist flow rate is greater than 15% for the 50 μm droplet and 10% for 80 μm droplet. The survival range for the wake flame, is a little greater than that for the envelope flame. Under the same mist flow rate, the smaller the droplets, the stronger the flame.

Finally, the effects of varying droplet size were studied by changing the droplet size and corresponding mist flow rate with the number flow rate constant. In this case study, 50 μm droplets with 5% mist flow rate were adopted as the initial droplet size and mist flow rate. As the droplet size was increased up to 55 μm, with a 6.655% corresponding mist flow rate, the envelope flame would be extinguished. The droplet size and corresponding mist flow for extinction were reasonable values to the previous study. For the 70 μm droplet size, the wake flame was extinguished.

This study considered only the thermal effects of mist on the flame since the expression for chemical kinetics does not consider the contribution of OH radical from the presence of water vapor. The consideration to include OH radical in the chemical kinetics will be carried in the near future to investigate the competition between heat loss, dilution of fuel and oxygen concentrations, and reaction enhancement by adding OH radical. The effects of various droplet sizes in a flow field and larger sized droplets are also worth studying.

NOMENCLATURE

$\overline{B}$	Frequency factor for gas phase reaction
C_D	Drag coefficient
c_d	Specific heat of the droplet
C_p	Average specific heat
$\overline{D}$	Dimensional species diffusivity
Da	Damkohler number
$\overline{D}_x$	Air drag in x direction
$\overline{D}_y$	Air drag in y direction
f	Stoichiometric oxidizer/fuel mass ratio
f_w	Nondimensional fuel-ejection rate
h_{fg}	Latent heat of droplet vaporization
k^*	Thermal conductivity at T^*
Le	Lewis number, $\overline{\alpha}/\overline{D}$
$\overline{\dot{m}}$	Burning rate on the porous cylinder
m_d	Droplet mass
$\overline{\dot{m}}_d$	Mass generation rate related to droplet
$\overline{P}$	Pressure
Pr	Prandtl number, $\overline{\nu}/\overline{\alpha}$
$\overline{Q}$	Heat of combustion per unit mass of fuel
$\overline{\dot{Q}}_d$	Heat absorption rate related to droplet
R^0	Universal gas constant
Re	Reynolds number
Re_d	Droplet Reynolds number
$\overline{T}$	Temperature
$\overline{T}_\infty$	Ambient temperature
T_w	Nondimensional wall temperature
T^*	Reference temperature

$\bar{u}$	Velocity in x-direction
$\bar{v}$	Velocity in y-direction
v_w	Fuel injection velocity on the cylinder surface
$\bar{x}$	Distance along x-direction
$\bar{y}$	Distance along y-direction
Y_f	Mass fraction of fuel, ρ_f/ρ
Y_o	Mass fraction of oxidizer, ρ_o/ρ
Y_{H_2O}	Mass fraction of water vapor.
Greek	
α^*	Thermal diffusivity at T^*
$\bar{\mu}$	Dynamic viscosity
μ^*	Dynamic viscosity at T^*
$\bar{\rho}$	Density
ρ^*	Density at T^*
ρ_d	Density of the droplet substance
$\bar{\dot{\omega}}$	Reaction rate
Overhead	
—	Dimensional quantities
Superscript	
*	Reference state
Subscript	
f	Fuel
o	Oxidizer
H_2O	Water vapor
w	Surface of the porous cylinder
a	Ambient
wall	Chamber wall
in	Inflow position
out	Outflow position
rc	Reference
n, t	Normal and tangential to cylinder surface

References

Alpert, R. L. (1985). Numerical Modeling of the Interaction between Automatic Sprinkler Sprays and Fire Plumes, *Fire Safety Journal*, **9**, 157–163.

Bird, R. B., Stewart, W. E., and Lightfoot, E. N. (1960). Transport Phenomena, John Wiley & Sons, New York.

Chen, C. H., and Weng, F. B. (1990). Flame Stabilization and Blowoff Over a Porous Cylinder, *Combustion Science and Technology*, **73**, 427.

Chen, N.-H., Rogg, B., and Bray, K. N. C. (1992). Modelling Laminar Two-phase Counterflow Flames with Detailed Chemistry and Transport, Twenty-fourth Symposium (International) on Combustion, The Combustion Institute, Pittsburgh, p. 1513–1521.

Chow, W. K. and Fong, N. K. (1993). Application of Field Modeling Technique to Simulate Interaction of Sprinkler and Fire-Induced Smoke Layer, *Combustion Science and Technology*, **89**, 101–151.

Crowe, C. T., Sharma, M. P., and Stock, D. E. (1977). The Particle-Source-In Cell Model for Gas-Droplet Flows, *Journal of Fluid Engineering*, **99**, 325–332.

Faeth, G. M. (1977). Current Status of Droplet and Liquid Combustion, *Progress in Energy and Combustion Science*, **3**, 191–224.

Gann, R. G., Editor (1995). Fire Suppression System Performance of Alternative Agents, NIST SP 890.

Grosshandler, W. L., Yang, J. C., and Cleary, T. G (1996A). Screening Method for New Fire Suppression Technologies, Proceeding of 1996 Conf. on Ozone Protection Technology, Washington, D. C..

Grosshandler, W. L., Yang, J. C., and Cleary, T. G. (1996B). Aerosol and SPGG Technology for Fire Research, NISTIR 5904.

Jicha, M., Karki, K. C., and Patankar, S. V. (1994). Numerical Analysis of Water Spray System in the Entrance Region of a Two-Dimensional Channel Using Lagrangian Approach, *Numerical Heat Transfer, Part A: Applications*, **26**, 1, 1–16.

Jones, A., and Nolan, P. F. (1995). Discussions on the Use of Fine Water Sprays or Mists for Fire Suppression, *J. Loss Prev. Process Ind.*, **8**, 1, 17.

Kim, M. B., Jang, Y. J., and Kim, J. K. (1996). Burning Rate of a Pool Fire with Downward-directed Sprays, *Fire Safety Journal*, **27**, 37–48.

Kim, M. B., Jang, Y. J., and Yoon, M. O (1997). Extinction Limit of a Pool Fire with a Water Mist, *Fire Safety Journal*, **28**, 295–306.

Liu, C. C., Lin, T. H., and Tien, J. H. (1993). Extinction Theory of Stretched Premixed Flames by Inert Sprays, *Combustion Science and Technology*, **91**, 309–327.

Liu, Q-C (1992). Studies on Flame Extinction in Two-phase Combustible Flows, Ph. D. Thesis, National Cheng Kung University, Taiwan.

Magee, R. S. and Reitz, R. D. (1986). Extinguishment of Radiation Augmented Plastic Fires by Water Sprays, Twenty-first Symposium (International) on Combustion, The Combustion Institute, Pittsburgh, p. 337–347.

Michaelides, E. E. (1997). Review-The Transient Equation of Motion for Particles, Bubbles, and Droplets, *Journal of Fluid Engineering*, **119**, 233–247.

Papadakis, S. E. and King, C. J. (1988A). Air Temperature and Humidity Profiles in Spray Drying. 1. Features Predicted by the Particle Source in Cell Model, *Industrial and Engineering Chemistry Research*, **27**, 2111–2116.

Papadakis, S. E. and King, C. J. (1988B). Air Temperature and Humidity Profiles in Spray Drying. 2. Experimental Measurements, *Industrial and Engineering Chemistry Research*, **27**, 2116–2123.

Patankar, S. V. (1980). Numerical Heat Transfer and Fluid Flow, Hemisphere, London.

Sirignano, W. A. (1983). Fuel Droplet Vaporization and Spray Combustion Theory, *Progress in Energy and Combustion Science*, **9**, 291–322.

Suh, J. and Atreya, A. (1995). The Effect of Water Vapor on Radiative Counterflow Diffusion Flames, *Proceedings of the ASME Heat Transfer Division*, **317–2**, 53.

Tsuji, H. and Yamaoka, I. (1967). The Counterflow Diffusion Flame in the Forward Stagnation Region of a Porous Cylinder, Eleventh Symposium (International) on Combustion, The Combustion Institute, Pittsburgh, p. 979.

Tsuji, H. (1982). Counterflow Diffusion Flame, *Progress in Energy and Combustion Science*, **8**, 93.

Wallis, G. B. (1969). One-Dimensional Two-Phase Flow, McGraw-Hill, New York.

Yang, J. C., Donnelly, M. K., Prive, N. C., and Grosshandler, W. L. (1999A). Fire Suppression Efficiency Screening Using a Counterflow Cylindrical Burner, Proceedings of the 5th ASME/JSME Joint Thermal Engineering Conference, AJTE99–6148, San Diego, California, March 15–19.

Yang, J. C., Donnelly, M. K., Prive, N. C., and Grosshandler, W. L. (1999B). Recent Results from the Dispersed Liquid Agent Fire Suppression Screen, Proceedings of the Halon Options Technical Working Conference Albuquerque, New Mexico, p. 27–29, April.

Yang, J. C., Donnelly, M. K., Prive, N. C., and Grosshandler, W. L. (1999C). Dispersed Liquid Agent Fire Suppression Screen Apparatus, National Institute of Standards and Technology, NISTIR 6319, 1999.